Light-driven extracellular electron transfer accelerates microbiologically influenced corrosion by Rhodopseudomonas palustris TIE-1

Lou, Yuntian; Zhang, Hao; Li, Ziyu; Liu, Shaopeng; Chang, Weiwei; Qian, Hongchang; Hao, Xiangping; Zhang, Dawei

Important note
To cite this publication, please use the final published version (if applicable).
Please check the document version above.

Corrosion Science

Light-driven extracellular electron transfer accelerates microbiologically influenced corrosion by *Rhodopseudomonas palustris* TIE-1

Yuntian Lou [a,b,c,1], Hao Zhang [a,b,1], Ziyu Li [d], Shaopeng Liu [a,b], Weiwei Chang [a,b], Hongchang Qian [a,b,c], Xiangping Hao [a,b], Dawei Zhang [a,b,c,*]

[a] *Beijing Advanced Innovation Center for Materials Genome Engineering, Institute for Advanced Materials and Technology, University of Science and Technology Beijing, Beijing 100083, China*
[b] *National Materials Corrosion and Protection Data Center, University of Science and Technology Beijing, Beijing 100083, China*
[c] *BRI Southeast Asia Network for Corrosion and Protection (MOE), Shunde Innovation School, University of Science and Technology Beijing, Foshan 528399, China*
[d] *Delft University of Technology, Department of Materials Science and Engineering, Mekelweg 2, Delft 2628CD, the Netherlands*

ARTICLE INFO

ABSTRACT

This study investigates the microbiologically influenced corrosion (MIC) of X80 steel accelerated by the phototrophic bacterium *Rhodopseudomonas palustris* TIE-1. The photorespiration plays a key role in promoting extracellular electron transfer (EET)-induced MIC. In the early corrosion stage, unstable localized corrosion dominated in the dark, while intense diffusion-controlled corrosion occurs in light. Compared to the sterile anaerobic medium, *R. palustris* TIE-1 accelerated corrosion of X80 steel, with a significantly higher corrosion rate under light conditions, approximately three times that of dark conditions. Inhibition of photosynthetic electron transfer or cessation of photostimulation resulted in pronounced reduction in the corrosion rate.

1. Introduction

Microbiologically influenced corrosion (MIC) denotes the accelerated degradation of materials caused by microbial activities and corrosive byproducts generated through microbial metabolism [1–3]. Microorganisms and their biofilms possess the capability to modulate properties at the solution/metal interface, influencing factors such as ion concentration, oxygen levels, and pH, subsequently impacting corrosion behaviors [4,5]. Additionally, microbes can generate corrosive metabolites, including various organic acids and corrosive gases [6,7]. In recent years, extracellular electron transfer (EET) induced microbial corrosion of metals has been identified as another pivotal MIC mechanism [8,9]. Microorganisms actively intervene in corrosion via EET to meet their own metabolic needs, rather than simply changing the interface environment.

EET refers to the process in which microorganisms transfer electrons either from the extracellular space to the intracellular environment or vice versa, typically involving solid electrodes or electron shuttles [10,11]. This mechanism contributes to microorganisms in survival and metabolism, particularly in extreme environments characterized by nutrient scarcity and anaerobic conditions. Currently, the majority of research has consistently indicated that microorganisms accelerate metallic corrosion through inward EET, also known as the biocathode process. For example, Venzlaff et al. compared the cathodic reactions of *Desulfovibrio corrodens* strain IS4 (corrosive SRB) and *Desulfovibrio* sp. strain HS3 (non-corrosive, H_2-consuming SRB) on pure iron as the sole electron donor [12]. The results confirmed that SRB accelerate cathodic reactions, promoting MIC via direct electron uptake, not through H_2 consumption to produce corrosive H_2S. Huang et al. found that *Pseudomonas aeruginosa*, under organic carbon starvation, utilized the electron shuttle pyocyanin to extract electrons from X80 steel, accelerating its corrosion. After the knockout of the gene for pyocyanin secretion, the corrosion of X80 steel decreased by approximately 48 % in the *P. aeruginosa* mutant [13]. Additionally, the outward EET process, in which microorganisms transfer electrons from inside the cell to outside using extracellular oxidants or solid electrodes, may also contribute to acceleration of corrosion. Hu et al. demonstrated that *Bacillus subtilis* utilized the passive film on 304 stainless steel as an alternative electron acceptor, leading to its degradation in the NO_3^--limited environment [14].

---

* Corresponding author at: Beijing Advanced Innovation Center for Materials Genome Engineering, Institute for Advanced Materials and Technology, University of Science and Technology Beijing, Beijing 100083, China.
  E-mail address: dzhang@ustb.edu.cn (D. Zhang).
  [1] These authors contributed equally to this work.

Rhodopseudomonas palustris TIE-1, a rod-shaped, Gram-negative purple non-sulfur bacterium, is a typical phototrophic bacterium found in ecosystems such as soils, sediments and water bodies. It is renowned for its ability to accept electrons from a variety of electron donors, including external electrodes (iron, carbon, conductive minerals, etc.), electron shuttles (quinone compounds, etc.), or other bacteria [15–19]. In the process of photorespiration, *R. palustris* TIE-1 converts light energy into chemical energy, elevating intracellular electrons to a higher energy state. This initiates the photosynthetic electron transport chain (PETC) and accelerates ATP synthesis, promoting the formation of a transmembrane proton gradient and an electrochemical potential difference. These processes collectively enhance EET [20,21]. Bose et al. demonstrated the capability of *R. palustris* TIE-1 to accept exogenous electrons [22]. With CO_2 as the sole carbon source/electron acceptor, *R. palustris* TIE-1 could uptake electrons from solid electrodes under light and dark conditions. While the photorespiration operated independently of the electron uptake system, it intensified the process of electron uptake. Rengasamy et al. explored strategies to enhance electron uptake in photoautotrophy conditions, leveraging *R. palustris* TIE-1's capability to directly utilize solid-state electrons as electron donors [23]. The results indicated that the addition of soluble ferrous iron did not enhance direct electron uptake, whereas on Prussian blue (PB) immobilized electrodes, the electron uptake by *R. palustris* TIE-1 was enhanced, with the cathodic current density increasing by approximately 3.8 times. The above studies demonstrated that *R. palustris* TIE-1 exhibited electron uptake from the environment and affinity to iron precipitates, resembling inward EET in MIC. However, the impact of light stimulation and microbial photorespiration on MIC mechanisms had not been reported.

In this study, we investigated for the first time the role of bacterial photorespiration in EET-MIC. The photosynthetic electron transport functions as a continuous driving force for inward EET under light conditions. During the 14-day anaerobic immersion, the surface morphology and roughness analysis of X80 steel were evaluated using scanning electron microscopy (SEM) and confocal laser scanning microscopy (CLSM). The composition of surface products was analyzed by X-ray photoelectron spectroscopy (XPS). The MIC behaviors of X80 steel were assessed through weight loss tests and electrochemical measurements, including linear polarization resistance (LPR), potentiodynamic polarization curves and electrochemical impedance spectroscopy (EIS). The fluctuation trend of electrode potential and current recorded by electrochemical noise (EN) under alternating light and dark conditions, along with ICP-MS analysis before and after inhibiting photorespiratory chain, were employed to demonstrate the crucial role of photorespiration in promoting EET-MIC.

2. Experimental methods

2.1. Bacteria and media

The *R. palustris* TIE-1 strain, obtained from the Guangdong Microbial Culture Collection Center (GDMCC), was utilized in this study. Bacterial culture and MIC experiments were performed using YPMOPS medium (yeast extract, peptone and MOPS), composed of 3 g yeast extract, 3 g tryptone, 1 g ammonium sulfate, 1.62 g sodium succinate, 2.09 g MOPS (buffer used in cell culture, 3-morpholine propionic acid) in 1 L deionized water. The initial pH of the YPMOPS medium was adjusted to 7.0 ± 0.2. Prior to use, the medium was sterilized at 121 °C for 20 min in an autoclave (Panasonic, MLS-3781-PC). The initial concentration of the planktonic *R. palustris* TIE-1 was adjusted to 10^6 cfu/mL using a hemocytometer under a light microscope (Zeiss, Lab A1) at × 400 magnification [24]. Given the impact of oxygen on corrosion and the facultative anaerobic nature of *R. palustris* TIE-1, the media underwent deoxygenation treatment. All experiments (microbial cultivation, corrosion immersion, electrochemical measurements) under light conditions were conducted under a single 60 W incandescent light bulb

positioned at 25 cm above the culture medium [25]. The dark conditions refer to fully shielding the culture apparatus from light using aluminum foil. All microbial cultivation and corrosion experiments were conducted at 30 °C.

2.2. Materials and surface analysis

All tests employed X80 steel coupons with dimensions of 10 mm × 10 mm × 3 mm, the components of which were listed in Table 1. Before testing, the coupons underwent sequential abrasion with 240, 400, 600, 800 and 1000 grit abrasive papers, followed by rinsing with anhydrous ethanol and drying with nitrogen. The coupons were sterilized under ultraviolet light for 30 minutes before use [26]. The surface morphologies of X80 steel coupons before and after removing the corrosion products were observed using scanning electron microscopy (SEM, Zeiss Gemini 500). Corrosion products and the biofilm on coupon surfaces were removed using Clarke's solution, as described by ASTM G1–03 [27]. For biofilm observation, the pretreatment steps were as follows: the biofilm on the coupon was fixed with 2.5 % (v/v) glutaraldehyde at 4 °C overnight and dehydrated with a gradient of ethanol solutions (50, 70, 90, 95, and 100 vol%). To enhance the conductivity of surface products, the coupons were sputtered with Au before SEM observation. To investigate the effect of *R. palustris* TIE-1 on X80 steel corrosion, energy dispersive spectrometer (EDS, Zeiss Gemini 500) and X-ray photoelectron spectroscopy (XPS, ESCALAB 250Xi) were used to analyze the composition of the surface products. Confocal laser scanning microscopy (CLSM, Kenyence VK-X260 K) was conducted to examine the morphology and surface roughness of coupons after removing surface products.

2.3. Electrochemical measurements

The electrochemical measurements were performed using an electrochemical workstation (Gamry, Reference 600 Plus). A three-electrode system was employed, consisting of an X80 steel coupon as the working electrode, a platinum foil as the counter electrode (CE), and a saturated calomel electrode (SCE) as the reference electrode. To ensure measurement stability, the open circuit potential (OCP) was performed for no less than 10 minutes before each electrochemical test. The polarization resistance (R_p) was obtained by measuring the linear polarization resistance (LPR) in the potential range from −10 mV to +10 mV vs. the E_{OCP} at a scan rate of 0.125 mV/s. Electrochemical impedance spectroscopy (EIS) measurements were conducted with a sinusoidal perturbation of 10 mV in a frequency range from 10^{-2} to 10^5 Hz. The potentiodynamic polarization curves were obtained by scanning the potential range from −200 mV to 200 mV vs. E_{OCP} after 14-day immersion tests, with a scan rate of 0.167 mV/s. The corrosion current density (i_{corr}) was determined using the Tafel extrapolation fitting method. Electrochemical noise (EN) measurements were performed using two nominally identical electrodes to record their potential and current in sterile and *R. palustris* TIE-1-inoculated (10^8 cfu/mL) media under alternating light/dark conditions, utilizing the ZRA mode with a sampling rate of 5 Hz [28,29]. Wavelet analysis was employed as a time-frequency method for trend removal [30].

2.4. Weight loss and ICP-MS

The weight loss analysis was conducted using an electronic balance (ME204, Mettler Toledo, precision ± 0.1 mg), with a minimum of 3 coupons used for each weight loss data point. Before immersion, the initial weights of the X80 carbon steel coupons were recorded. After immersion, the surface products were removed using Clarke's solution, as described by ASTM G1–03. Subsequently, the coupons with removed surface products were cleaned using anhydrous ethanol, dried with nitrogen, and reweighed [31]. In the immersion tests, rotenone, at a working concentration of 6 μM, was added to inhibit the photosynthetic

Table 1
Chemical composition (wt%) of X80 steel.

Elements	C	Si	Mn	Cr	Mo	Ni	Cu	Nb	Fe
wt%	0.07	0.24	2.16	0.31	0.35	0.41	0.25	0.15	balanced

electron transfer chain of *R. palustris* TIE-1 [32]. To confirm the promoting effect of *R. palustris* TIE-1 photorespiration on X80 steel corrosion, iron release was determined using ICP-MS (Thermo Scientific, iCAP TQs).

3. Result and discussion

3.1. Bacterial growth and pH variation

Fig. 1 shows the variation in the growth characteristics of *R. palustris* TIE-1 under both light and dark conditions over the 14-day incubation period. In the Fig. 1a, the growth curves of planktonic *R. palustris* TIE-1 was recorded. Under light/dark conditions, the cell number of *R. palustris* TIE-1 exhibited an initial increase followed by a gradual decrease throughout the culture cycle. In the presence of light, *R. palustris* TIE-1 reached a peak concentration of approximately 10^9 cells/mL after 4 days. While under dark conditions, the growth rate of *R. palustris* TIE-1 was relatively slow, reaching a peak concentration of planktonic cells of $\sim 7 \times 10^8$ cells/mL after 6 days. Subsequently, the cell numbers decreased gradually under both conditions to $\sim 4 \times 10^8$ cells/mL after 14 days. Notably, under light conditions, the *R. palustris* TIE-1 medium appeared red due to pigment production (carotenoids) under anaerobic light stimulation, which enhanced photorespiration efficiency and may explain its high activity [33–35]. Fig. 1b shows the variation of pH value in the media over 14 days period under different conditions. Regardless of light and dark conditions, the pH values of the culture media were very stable within 14 days, at approximately 8.5 and 7.5, respectively. The pH difference was attributed to variation in metabolic rates, leading to differences in metabolites accumulation [36]. The above results indicated that during 14-day culture period, *R. palustris* TIE-1 exhibited stable growth and metabolism, with higher activity under light conditions [37].

3.2. Surface morphology

Fig. 2 shows the morphology of biofilm and corrosion products on the X80 steel in the sterile medium under light and dark conditions. In the sterile medium (Fig. 2a), almost no corrosion occurred, and the

grinding marks on coupon surfaces were clearly visible. After 14 days (Fig. 2b-b₁), the coupon surface morphology was almost unchanged, with only localized appearance of a small amount of corrosion products. In the medium inoculated with *R. palustris* TIE-1 under light conditions, the coupon surface was uniformly attached with bacterial cells. By the 7th day, *R. palustris* TIE-1 tended to aggregate and form clusters (Fig. 2c). After 14 days, a small part of the bacteria agglomerated into larger clusters, indicating the formation of a mature biofilm on the coupon surface (Fig. 2d). Under dark conditions, *R. palustris* TIE-1 on the coupon surfaces experienced a similar process of uniform adhesion (Fig. 2e), forming clusters by the end of the 14 days (Fig. 2f). Notably, significant differences in biofilm morphology between light and dark conditions were observed on the 14th day (Fig. 2d₁ vs. Fig. 2f₁). Under light conditions, although the *R. palustris* TIE-1 cells attached to the coupon surface still exhibited the original rod-like shape, their cell walls were completely covered by irregular particles. However, wrinkled cell wall without irregular particles was observed on the coupon surface under the dark conditions, indicating no additional accumulation of corrosion products other than biofilm attachment. The EDS results demonstrated a significantly higher oxygen content on the sample surface under light conditions compared to the other two conditions, implying that corrosion products accumulated most prominently under light conditions.

Fig. 3 shows the surface morphology of the X80 steel after removing the surface products under different conditions, which is used to evaluate the degree of corrosion. As illustrated in Fig. 3a-c, after 7 days of immersion, the surface morphology of coupons under sterile and dark conditions exhibited similarity, with a small number of pits. The overall corrosion was mild, and traces of the abrasion during pretreatment were still visible. However, noticeable corrosion was evident on the coupon surface under light conditions, where abrasion marks had nearly disappeared, and larger pits appeared locally (Fig. 3b₁). After 14 days, the surface morphology under sterile conditions remained almost unchanged (Fig. 3d-d₁), indicating that the sterile medium had no obvious promoting effect on corrosion. The coupon surfaces exhibited increased corrosion under *R. palustris* TIE-1-inoculated media after 14 days. Under light conditions (Fig. 3e-e₁), the coupon surface became rougher, and larger pits were observed. Under dark conditions (Fig. 3f-f₁), the coupon
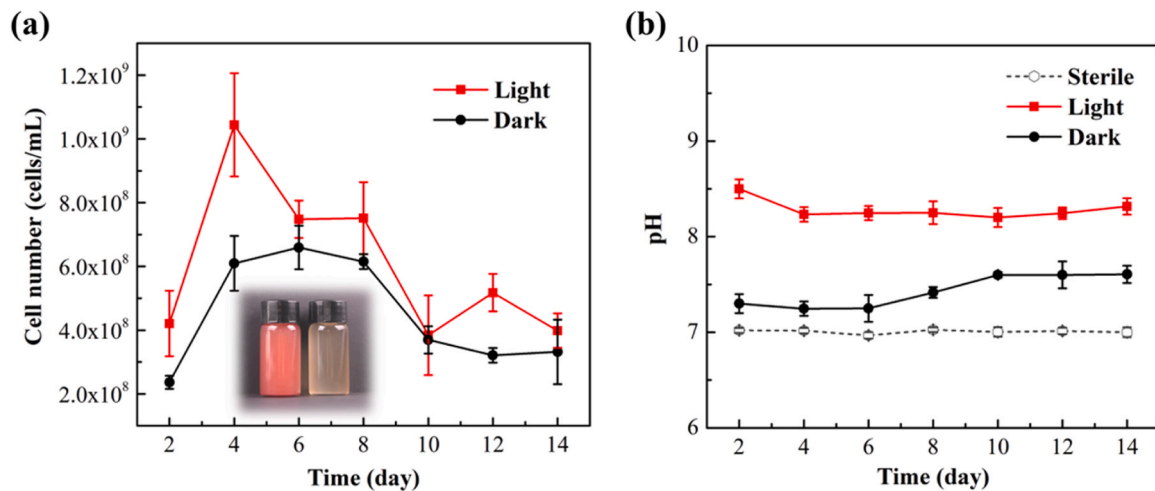

Fig. 1. (a) Growth curves of *R. palustris* TIE-1 under light and dark conditions for 14 days; (b) The pH variation of *R. palustris* TIE-1 under different conditions for 14 days.
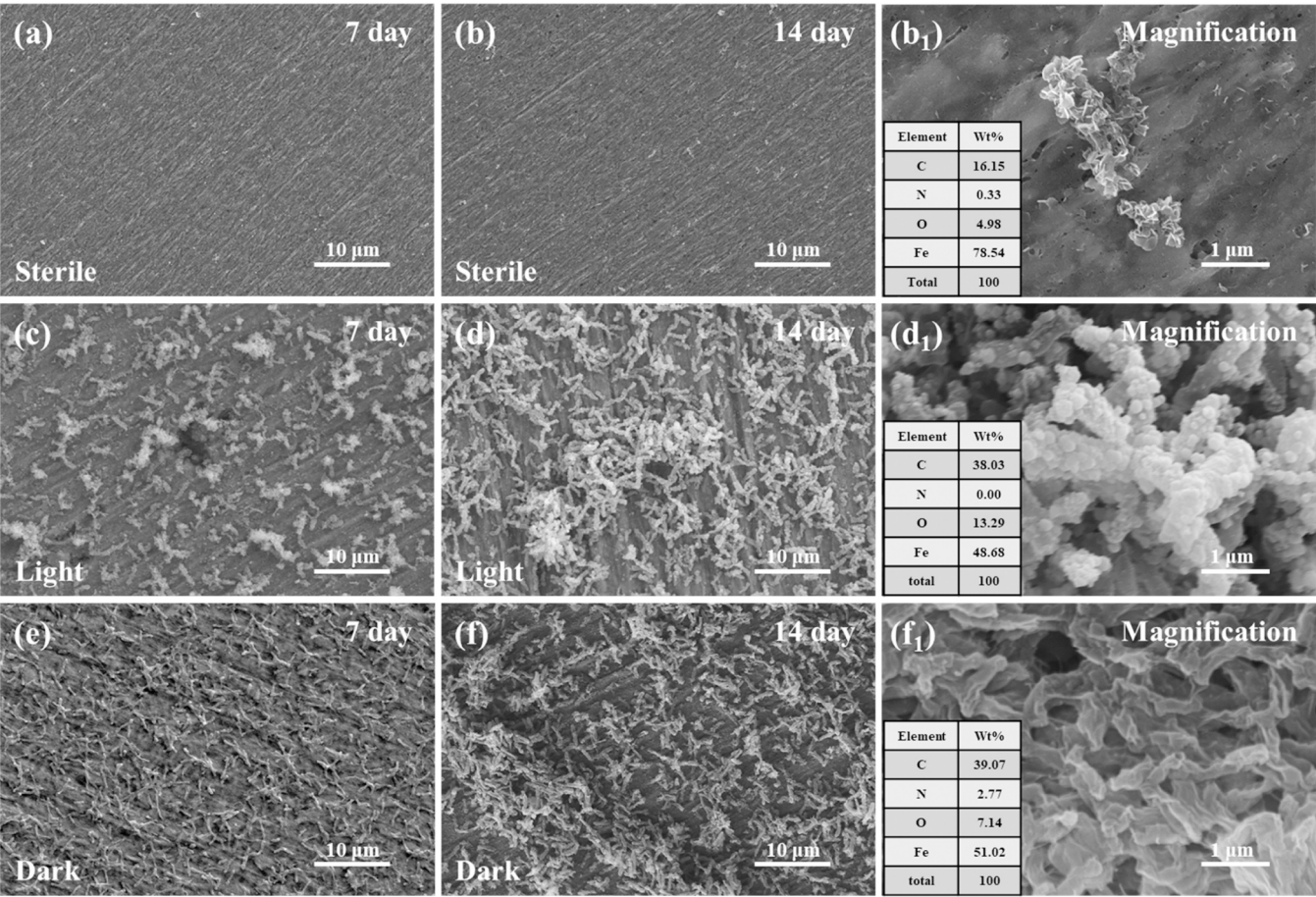
Fig. 2. SEM images of the X80 steel surfaces: (a, b) in the sterile media, (c, d) under *R. palustris* TIE-1 inoculation in light conditions, and (e, f) under *R. palustris* TIE-1-inoculation in dark conditions on the 7th day and 14th day, respectively; (b₁, d₁, f₁) surface magnification and EDS results for each condition on the 14th day.
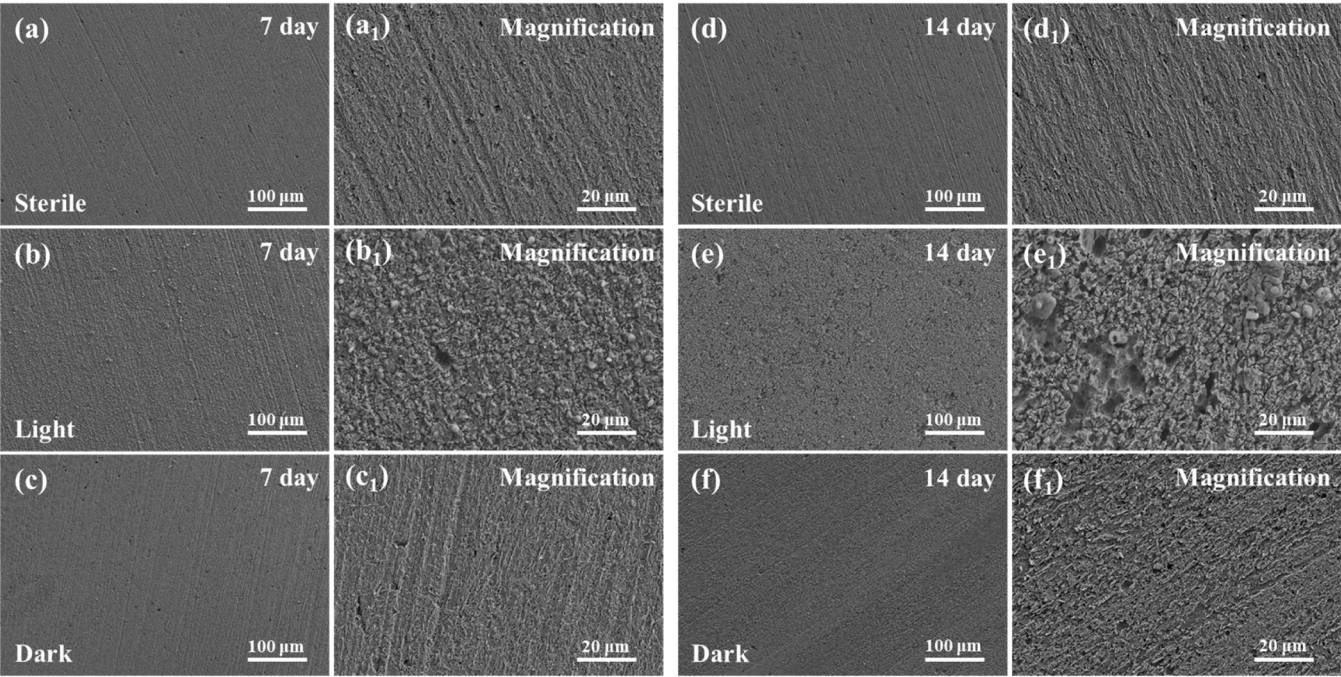

Fig. 3. SEM images of X80 coupons after surface product removal. (a, d) sterile media for 7 and 14 days; (b, e) *R. palustris* TIE-1-inoculated media under light conditions for 7 and 14 days; (c, f) *R. palustris* TIE-1-inoculated media under dark conditions for 7 and 14 days; (a₁, b₁, c₁, d₁, e₁, f₁) corresponding enlarged images.

surface showed a small number of pits and uniform corrosion. These results indicated that *R. palustris* TIE-1 could accelerate corrosion of X80 steel, with light further promoting this process.

To further assess the degree of corrosion under different conditions, CLSM was employed to analyze the surface roughness after 14 days of immersion. The "five-point sampling method" was utilized to select five areas on the coupon surface (based on the CLSM images, Fig. 4a-c), and the surface roughness Sa (arithmetical mean height) was statistically analyzed [38]. As shown in Fig. 4d, the average Sa values for coupons after 14 days of immersion were 0.3 μm under sterile conditions, 1.5 μm under inoculated conditions with light, and 0.4 μm under inoculated conditions with darkness. The t-test results indicated significant differences in roughness values among the sterile, light, and dark conditions. Notably, the roughness under light conditions was significantly higher than in the other two conditions. This suggested that *R. palustris* TIE-1 promoted corrosion, and this corrosion phenomenon was more pronounced under light conditions.

3.3. Weight loss measurements

Fig. 5 illustrates the weight loss of the X80 steel coupons in the sterile, *R. palustris* TIE-1-inoculated media under light/dark conditions after 3, 7 and 14 days. The results showed that the average weight loss rate in the *R. palustris* TIE-1-inoculated medium was significantly higher than the other two conditions at any sampling point under light conditions. After 3 days, the average weight loss values of the coupons in sterile conditions, *R. palustris* TIE-1-inoculated media under light/dark conditions were 0.3 mg/cm^2, 1.5 mg/cm^2, and 0.7 mg/cm^2, respectively. The statistical analysis results showed significant differences in weight loss between the inoculated and the sterile conditions, while there was no difference between the light and dark conditions. After 7 days, the average weight loss values of the coupons in sterile, *R. palustris* TIE-1-inoculated media under light/dark conditions were 0.6 mg/cm^2, 3.1 mg/cm^2 and 1.1 mg/cm^2, respectively. The above variation trend
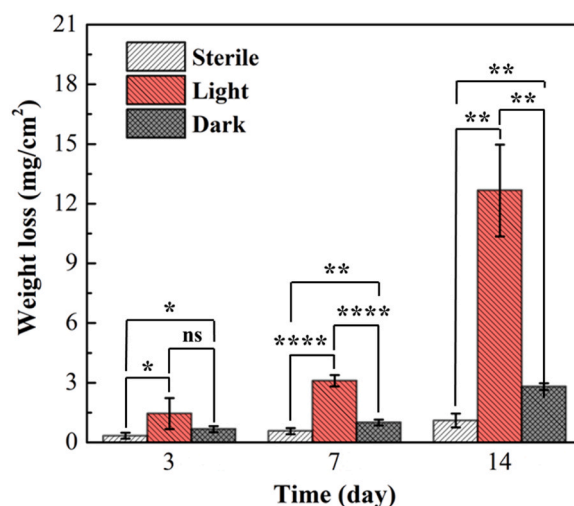

Fig. 5. Weight loss of X80 coupons after 3, 7 and 14 days of immersion in different conditions; statistical analyses were determined by t-test using a two-tailed test: * $p < 0.05$; ** $p < 0.01$; *** $p < 0.001$; **** $p < 0.0001$.

suggested that corrosion under the sterile medium and the inoculated medium under dark conditions was limited, while the coupon corrosion was significantly aggravated in the inoculated medium under light conditions. With further immersion time extended to 14 days, the average weight loss value of coupons in the *R. palustris* TIE-1 inoculated medium under light conditions further increased to 12.7 mg/cm^2, which was over 3 times higher than that on the 7th day. The average weight loss under the sterile and the dark conditions also increased after 14 days, but rate of the increase was much lower than that under light conditions.

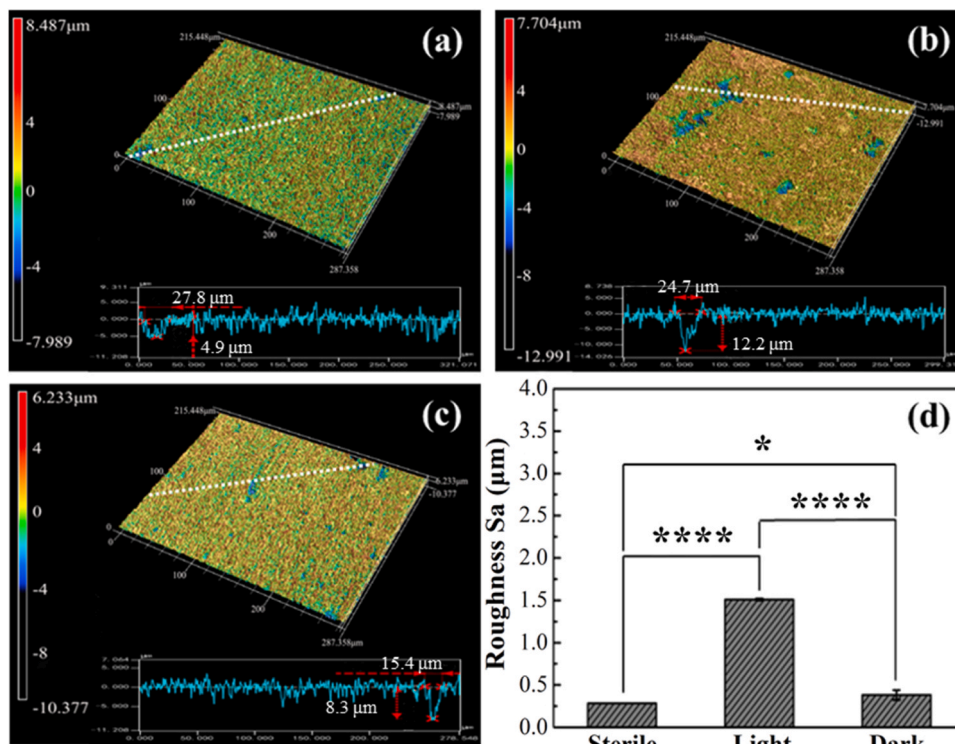**Fig. 4.** CLSM images of X80 coupons after the removal of the surface products formed after 14 days of immersion under different conditions. (a, b, c) in the sterile, *R. palustris* TIE-1-inoculated media under light/dark conditions, respectively; (d) the average surface roughness analysis; statistical analyses were determined by t-test using a two-tailed test: * $p < 0.05$; ** $p < 0.01$; *** $p < 0.001$; **** $p < 0.0001$.

3.4. XPS analysis

Fig. 6 shows the high-resolution XPS spectra of Fe and O on the X80 steel surface after 14 days of immersion, including deconvolution results and the calculated proportions of different components. In Fig. 6a, the Fe $2p_{3/2}$ spectrum consisted of peak components with binding energies at 713.1 eV, 711.1 eV, and 709.7 eV, which were attributed to FeOOH, Fe_2O_3 and Fe_3O_4 [39,40]. When calculating Fe^{2+} and Fe^{3+} percentages, Fe_3O_4 is considered equivalent to $FeO \cdot Fe_2O_3$ [41]. Compared to the sterile condition, the proportion of iron hydroxide on the surfaces of coupons under light and dark conditions decreased, and more iron oxides were produced. Notably, the Fe^{2+}/Fe^{3+} ratio under light conditions was markedly lower than that under sterile condition, indicating an enhanced oxidation of Fe^{2+} to Fe^{3+}. Under dark conditions, the Fe^{2+}/Fe^{3+} ratio was higher than that of the sterile condition, suggesting an accumulation of more Fe^{2+} in the coupon surface products without further oxidation to Fe^{3+}. In Fig. 6b, the O 1s spectrum consisted of peak components with binding energies at 532.4 eV, 531.1 eV, 530.7 eV and 529.6 eV, corresponding to H_2O, OH, organic O and O^{2-}. The OH peaks were attributed to EPS and iron hydroxide, while the O^{2-} peaks were attributed to iron oxides [42]. In the corrosion process of X80 steel involving *R. palustris* TIE-1, the proportion of O^{2-} exceeded that under the sterile condition, especially under light conditions. The above results indicated that light promoted the corrosion of X80 steel by *R. palustris* TIE-1, corresponding to both morphological observations and weight loss data.

3.5. Electrochemical measurements

To further elucidate the impact of light/dark conditions on the corrosion behavior of X80 steel by *R. palustris* TIE-1, the electrochemical tests were employed. Fig. 6a shows the $1/R_p$ values obtained from LPR tests on X80 steel coupons immersed in sterile, *R. palustris* TIE-1-inoculated media under light/dark conditions for 14 days. $1/R_p$ is positively correlated with the corrosion rate [43]. Throughout the immersion cycle, the $1/R_p$ values remained stable and at a low level under sterile and *R. palustris* TIE-1-inoculated medium under dark conditions. In contrast, the $1/R_p$ values under light conditions containing *R. palustris* TIE-1 remained consistently high with noticeable fluctuations. Notably, the $1/R_p$ values were significantly higher in the first 7 days compared to the subsequent 7 days, and this trend was similar to the corresponding growth curve under light conditions. This suggested a close relationship between bacterial activity and corrosion rate, indicating that the presence of *R. palustris* TIE-1 under light conditions significantly accelerated corrosion. Fig. 6b shows the potentiodynamic polarization curves of X80

steel coupons in the sterile, *R. palustris* TIE-1 inoculated media under light/dark conditions for 14 days. The electrochemical parameters for the X80 steel tested under different conditions are listed in Table 2, including corrosion current density (i_{corr}), corrosion potential (E_{corr}), cathodic (β_c) and anodic (β_a) Tafel slopes. As illustrated in Fig. 6b, the cathode branches of the potentiodynamic polarization curves almost overlapped under different conditions, while the anodic branches exhibited significantly differences. Especially under light conditions, the anodic branch shifted to the right, resulting in a lower E_{corr} (-794.1 mV) and a higher i_{corr} (2.4 µA cm^{-2}), which was three times that of other conditions. In contrast, the polarization curves under the sterile and dark conditions were similar, with the i_{corr} values of 0.7 µA cm^{-2} and 0.8 µA cm^{-2}, respectively. The above results demonstrated that light exposure was a key factor in corrosion acceleration of *R. palustris* TIE-1 on X80 steel. Under dark conditions, even if the medium was inoculated with *R. palustris* TIE-1, the effect of MIC was weak.(Fig. 7)

Fig. 8 shows the EIS results of X80 steel during a 14-day immersion period under different conditions. Typically, the diameter of the capacitive arc in the low-frequency range indicates the degree of difficulty in charge transfer at the electrode-medium interface. In Fig. 8a, under sterile conditions, the diameter of the capacitive arc in the low-frequency range increased significantly on the third day, followed by a stable trend with a slight increase. In the inoculated medium under light conditions (Fig. 8b), the diameters of capacitive reactance arcs were generally much smaller than those of the sterile condition. Throughout the initial 7 days of the immersion cycle, the capacitive reactance arc diameters consistently decreased, and then increased slightly. This phenomenon may result from a decrease in electron uptake efficiency due to reduced metabolic activity of *R. palustris* TIE-1 in the later stages. Contrastingly, in the inoculated medium under dark conditions (Fig. 8c), the fluctuation range of capacitive reactance arc diameters during the 14-day immersion cycle were similar to that observed under sterile conditions, indicating that *R. palustris* TIE-1 had a weakened effect on corrosion process in the absence of photostimulation.

Fig. 9 shows the electrochemical equivalent circuit to fit the EIS data.

Table 2
Tafel polarization parameters obtained from the polarization curves of X80 steel under different conditions.

	i_{corr} (µA cm^{-2})	E_{corr} (mV vs. SCE)	β_c (mV dec^{-1})	β_a (mV dec^{-1})
Sterile	0.7	−749.2	84.9	107.5
Light	2.4	−794.1	75.8	162.6
Dark	0.8	−747.4	76.4	129.2

(a)

Fe 2p

Sterile
FeOOH : 20.4%
Fe_2O_3 : 53.5%
Fe_3O_4 : 26.1%
$Fe^{2+}:Fe^{3+}$ = 0.09

Light
FeOOH : 18.6%
Fe_2O_3 : 67.6%
Fe_3O_4 : 13.8%
$Fe^{2+}:Fe^{3+}$ = 0.05

Dark
FeOOH : 14.6%
Fe_2O_3 : 46.8%
Fe_3O_4 : 38.6%
$Fe^{2+}:Fe^{3+}$ = 0.14

(b)

O 1s

Sterile
O^{2-} : 7.4%
OH : 63.0%
Organic O : 9.2%
H_2O : 20.4%

Light
O^{2-} : 19.2%
OH : 35.0%
Organic O : 7.8%
H_2O : 38.0%

Dark
O^{2-} : 10.7%
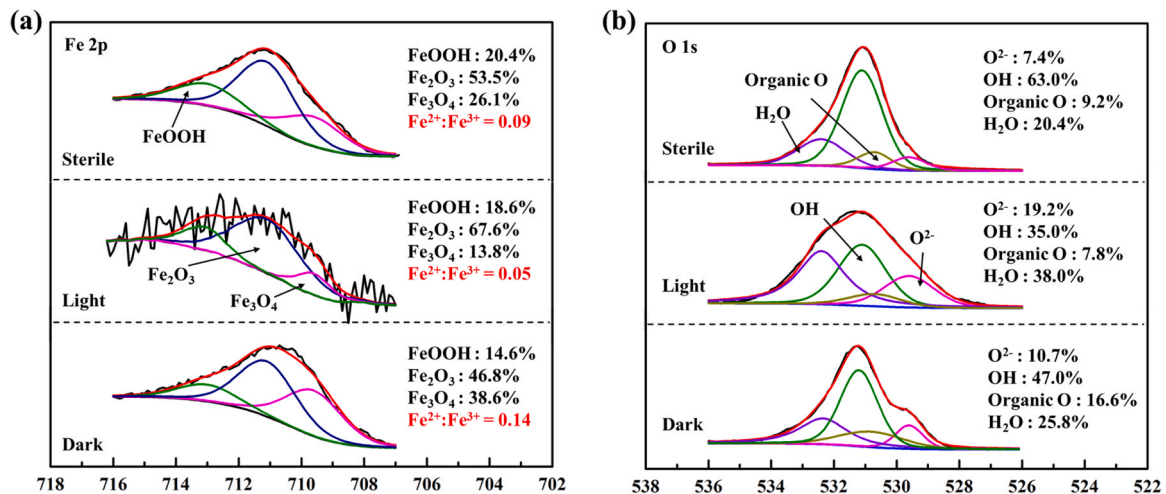OH : 47.0%
Organic O : 16.6%
H_2O : 25.8%

Fig. 6. High-resolution XPS spectra of Fe_{2p} and O_{1s} for the X80 steel surface after immersion in the different conditions for 14 days.
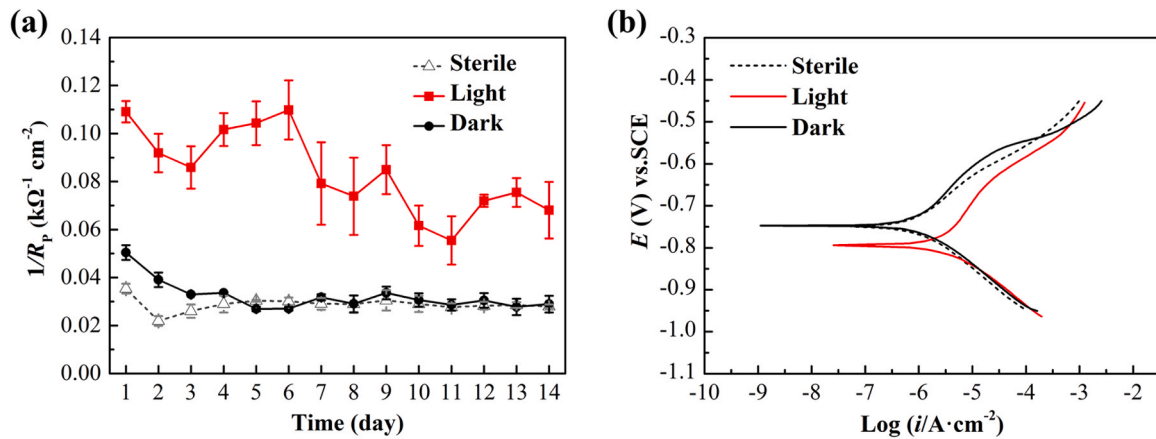
Fig. 7. (a) The $1/R_p$ variation and (b) potentiodynamic polarization curves of X80 coupons in the sterile, *R. palustris* TIE-1-inoculated media under light/dark conditions for 14 days.
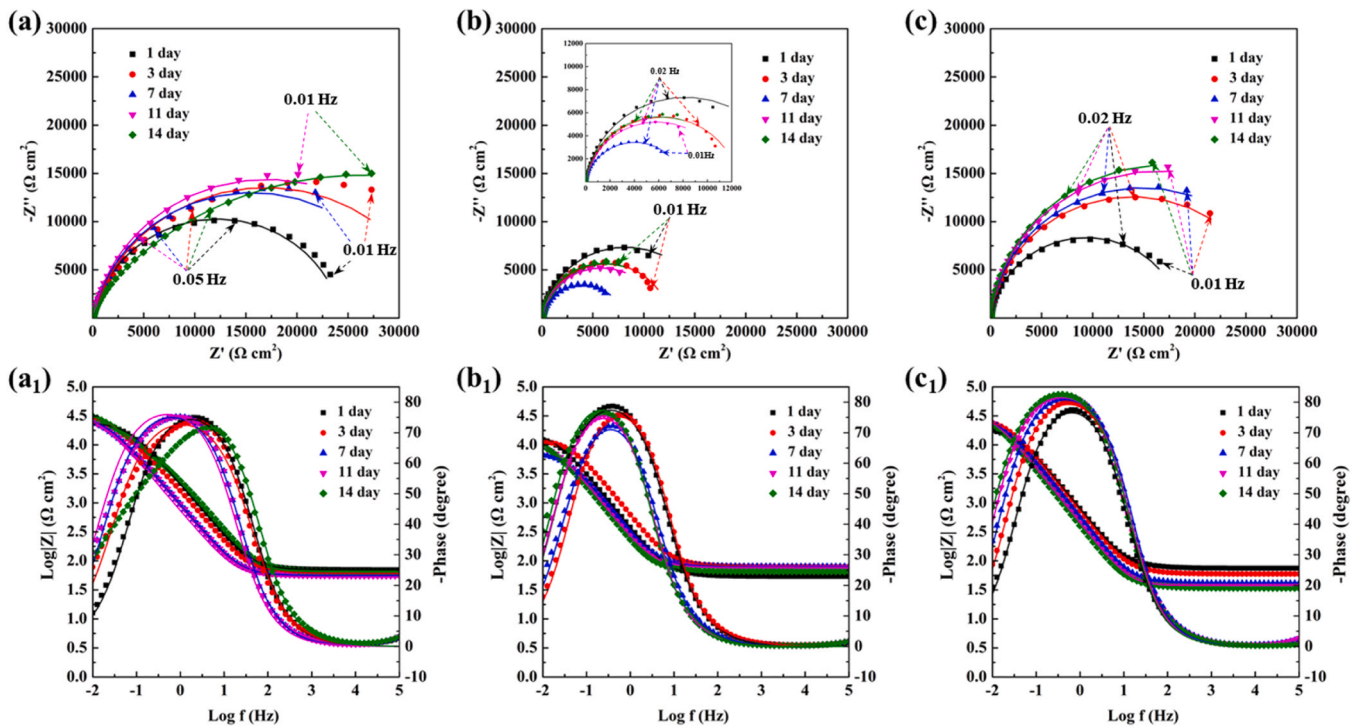

Fig. 8. Nyquist (a, b, c) and Bode plots (a₁, b₁, c₁) of the X80 steel coupons in the in the sterile (a, a₁), *R. palustris* TIE-1-inoculated media under light (b, b₁) and dark (c, c₁) conditions for 14 days.
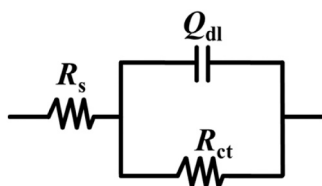

Fig. 9. Electrochemical equivalent circuits applied to fit the measured EIS data.

According to Fig. 2, the morphologies exhibited almost imperceptible corrosion product accumulation in sterile medium, and the biofilm did not completely cover the coupon surface in bacteria-inoculated medium. Notably, the biofilms typically have a water content exceeding 95 %, which means they do not exhibit impedance properties like organic coatings or corrosion product layers. Therefore, the one-time constant

model was employed for all conditions [44]. In this circuit, Q represents the constant phase element (CPE) and its impedance is calculated using Eq. (1),

$$Z_Q = Y_0^{-1}(j\omega)^{-n} \tag{1}$$

where Y_0 and n represent the characteristic parameters of CPE, and ω demotes the angular frequency. R_s is the solution resistance, R_{ct} is the charge transfer resistance, and Q_{dl} represent non-ideal capacitive behavior of the electrical double layer. The double layer capacitance (C_{dl}) was calculated using Eq. (2) introduced by Brug et al. [45].

$$C_{dl} = Q_{dl}^{1/n}(R_s^{-1} + R_{ct}^{-1})^{(n-1)/n} \tag{2}$$

Table 3 presents the corresponding fitting data of EIS. The R_{ct} values in both sterile medium and *R. palustris* TIE-1-inoculated medium (dark) consistently exhibited a gradual increase over time, suggesting that

Table 3
EIS parameters for X80 steel immersed in different conditions.

Time (day)	R_s (Ω cm^2)	$Q_{dl} \times 10^{-5}$ (Ω^{-1} cm^{-2} s^n)	n	$C_{dl} \times 10^{-5}$ (Ω^{-1} cm^{-2})	R_{ct} (kΩ cm^2)	$1/R_{ct}$ (kΩ^{-1} cm^{-2})
Sterile						
1	70.6	9.2	0.89	4.9	24.3	0.04
3	60.9	13.5	0.86	6.2	33.8	0.03
7	56.2	21.3	0.88	11.6	31.1	0.03
11	52.7	26.5	0.89	15.6	34.3	0.03
14	62.5	10.5	0.81	3.2	31.9	0.03
Light						
1	67.9	11.2	0.93	7.8	16.9	0.06
3	80.8	29.5	0.92	21.3	12.5	0.08
7	79.6	60.6	0.93	48.2	7.91	0.13
11	77.4	71.1	0.91	53.3	11.6	0.09
14	66.3	81.4	0.93	65.3	12.9	0.08
Dark						
1	75.9	22.8	0.93	16.8	18.6	0.05
3	60.5	24.4	0.94	18.6	27.7	0.04
7	41.5	31.8	0.94	24.1	29.5	0.03
11	37.7	38.4	0.96	32.2	33.2	0.03
14	34.9	43.7	0.81	16.4	34.4	0.03

corrosion products or deposits mixed with biofilm obstructed change transfer at the interface. Therefore, corrosion was generally mild under these conditions. The $1/R_{ct}$ can be used to reflect the corrosion rate [46]. The $1/R_{ct}$ values in the inoculated medium under light conditions were significantly higher than those under the other two conditions. This indicates an enhanced electrochemical activity at the interface, facilitating more efficient charge transfer. In particular, on the 14th day, the $1/R_{ct}$ value under light conditions is about 2.6 times the values under the sterile and dark conditions, the results that were highly consistent with the trend shown by i_{corr} values. The above results demonstrated that *R. palustris* TIE-1 under light stimulation accelerated corrosion of X80 steel.

The EN measurement was conducted to examine the impact of *R. palustris* TIE-1 on X80 steel corrosion under alternating light/dark conditions, leveraging its continuous, sensitive, and non-destructive characteristics [47,48]. Fig. 10 shows the potential and current signals obtained from the EN measurement under different conditions. Before data collection, all coupons were immersed in dark conditions for 2 hours to stabilize the coupon surface. In the sterile medium (Fig. 10a), both the potential and current values exhibited fluctuations, but their overall trend remained highly stable, unaffected by alternating light/-dark cycles. In contrast, the changes in the potential and current values in the inoculated medium exhibited highly sensitive responses to light/dark transitions (Fig. 10b). During the first 2 hours, the potential and current values remained relatively stable under dark conditions. Upon exposure to light (the 2nd to 4th hour), the potential immediately dropped and continued to decrease, accompanied by a rapid increase in current, which persisted until the end of the illumination. During the

subsequent 4 hours (the 4th to 8th hour), with alternating light on/off, the variation of the potential and current values is very similar to that observed in the initial 4 hours. The above results revealed that photo-stimulation did not affect the corrosion behavior of X80 steel under sterile condition However, in the inoculated medium, the influence of light on the potential and current signal of X80 steel was primarily attributed to the EET caused by *R. palustris* TIE-1 photorespiration.

Based on the results in Fig. 10, data collection was performed for 2000 s following the intermediate point of each cycle, designated as 1 h + 2000 s, 3 h + 2000 s, 5 h + 2000 s, and 7 h + 2000 s. Subsequently, the continuous wavelet transform (CWT) spectrum and energy distribution plot (EDP) of the EN potential signals of X80 steel were generated, facilitating the transient analysis of corrosion behavior under alternating light/dark conditions (Fig. 11 and Fig. 12). The EDP can provide valuable information about the predominant corrosion process according to the location of maximum relative energy at different stages and the relative energy changes of crystals [49–51]. It is generally accepted that the relative energy distributions in crystal d1-d3, d4–d6, and d7-d8 mainly reflect activation control, mixed control, and diffusion control [52–54].

In the inoculated medium, the relative energy under dark conditions was predominantly concentrated within crystals d1-d3 and d8, indicating that corrosion was primarily controlled by diffusion, with some localized corrosion (Fig. 11a$_1$). After illumination began, the maximum value (color scale) of the signal energy (Fig. 11b) was much higher than that under dark conditions. And the relative energy distribution was converged toward d8 (Fig. 11b$_1$), which indicated the transition of corrosion to a more stable, more severe state. When the illumination stopped, the relative energy distribution was redistributed from the low-frequency region to the high-frequency region (Fig. 11c$_1$), and the signal energy decreased (Fig. 11c). And then, the phenomenon in Fig. 11b-b$_1$ was repeated when the light was turned on again (Fig. 11d-d$_1$). Combined with the results of corrosion morphology (Fig. 3), it was demonstrated that *R. palustris* TIE-1 promoted localized corrosion under the light stimulation. In the sterile medium (Fig. 12), the maximum relative energy distribution in the first 2000 s was observed at d8 (Fig. 12a$_1$), while a small amount of energy was distributed among crystals at other locations. Over the subsequent three periods (Fig. 12b$_1$- d$_1$), the relative energy distribution gradually converged towards d8, with its changing trend exhibiting no correlation with alternations between light/dark conditions. Combined with the morphology results, it was evident that the corrosion of the coupon under sterile conditions was primarily characterized by uniform corrosion in the initial stage, with some weak localized corrosion. Ultimately, the localized corrosion almost stopped and was completely controlled by diffusion, with light/dark alternations showing no effect on the corrosion process in the absence of *R. palustris* TIE-1.

To elucidate the mechanism behind the photo-accelerated MIC of *R. palustris* TIE-1, we investigated the concentration of iron ions released from the corrosion of X80 steel after inhibiting light-driven EET of
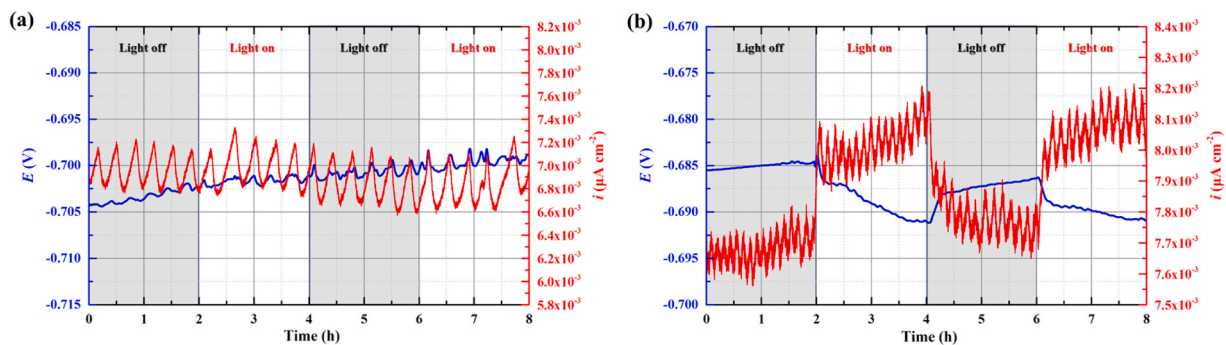

Fig. 10. The potential and current signals of X80 steel of EN measurements in (a) sterile and (b) *R. palustris* TIE-1-inoculated media under alternating light/dark conditions.
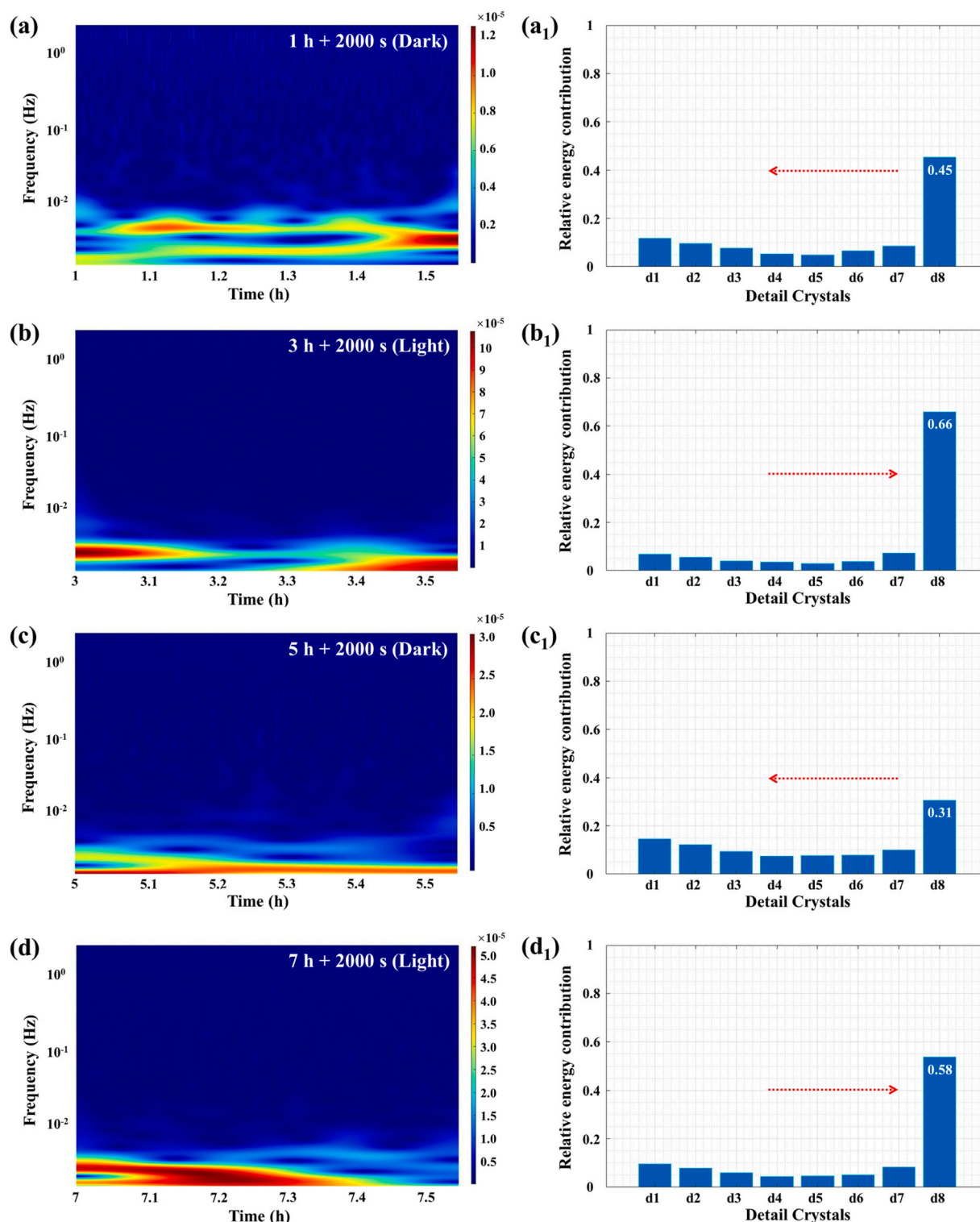
Fig. 11. CWT spectrum (a-d) and EDP (a₁-d₁) of EN potential signals for X80 steel immersed in *R. palustris* TIE-1-inoculated medium under alternating light/dark conditions.

R. palustris TIE-1 using rotenone (Fig. 13). Rotenone is an odorless, colorless, crystalline compound. As a targeted inhibitor, it can block the electron transport pathway between ubiquinone and NADH dehydrogenase in the photorespiratory chain, resulting in restriction or termination EET [55,56]. In the absence of rotenone, the highest concentration of iron ions was found in the inoculated medium after 14 days of light exposure. While the concentrations under the other two

conditions remained low, consistent with the weight loss results. However, in the medium with rotenone, the iron ion concentration under light conditions significantly decreased, almost reaching the level observed in the dark conditions. This indicated that inhibiting the photorespiratory chain weakened the driving force for *R. palustris* TIE-1 electron uptake, leading to a reduction in EET efficiency. Under dark conditions, the photorespiratory chain was not activated, the
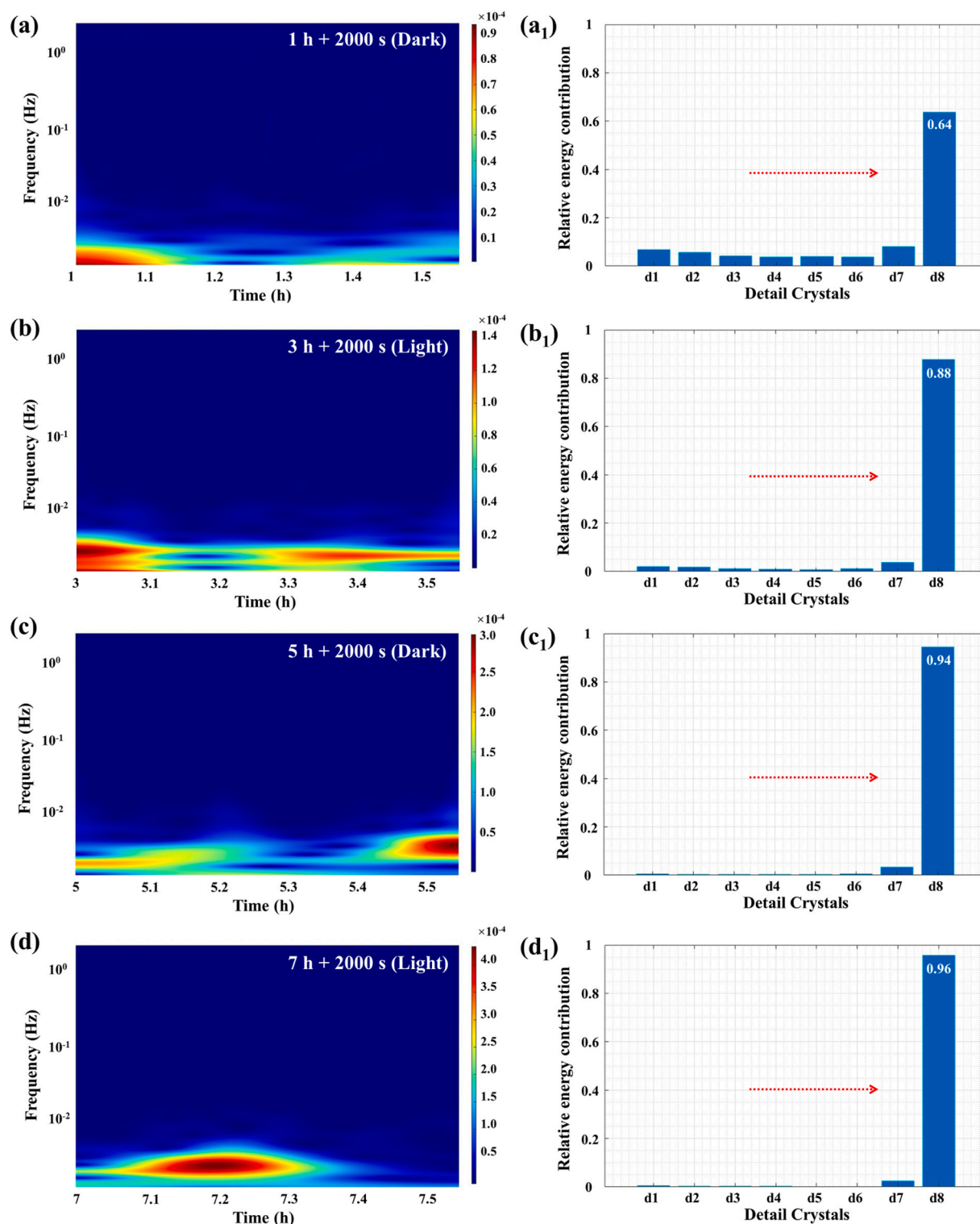
Fig. 12. CWT spectrum (a-d) and EDP (a₁-d₁) of EN potential signals for X80 steel immersed in the sterile medium under alternating light/dark conditions.

introduction of rotenone exerts no discernible influence on the concentration of released iron ions.

4. Conclusions

In summary, the mechanism of accelerating MIC of X80 steel by *R. palustris* TIE-1 photorespiratory process was investigated in this study. In contrast to sterile conditions, the corrosion of X80 steel was accelerated in the medium inoculated with *R. palustris* TIE-1, particularly under light condition. The light-driven EET-MIC behaviors of X80 steel were examined by surface morphology, weight loss, XPS, ICP-MS measurements and electrochemical analysis including LPR, potentiodynamic polarization curves and EN analysis. The main conclusions are as follows:
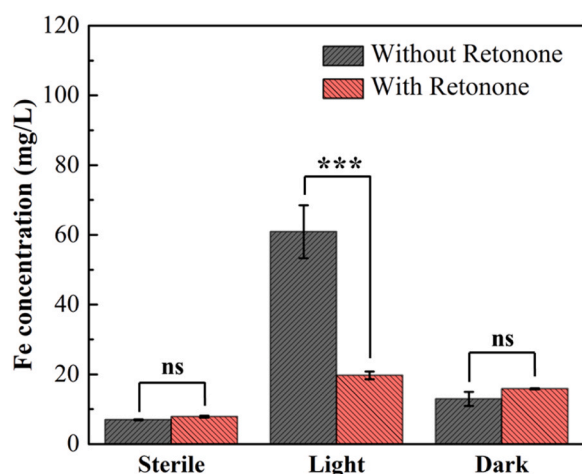
Fig. 13. ICP-MS results for the dissolved Fe in the different conditions for 14 days; statistical analyses were determined by t-test using a two-tailed test: * $p < 0.05$; ** $p < 0.01$; *** $p < 0.001$; **** $p < 0.0001$.

1. *R. palustris* TIE-1 promoted the corrosion of X80 steel in an anaerobic environment, exhibiting predominant localized corrosion under light conditions and uniform corrosion under dark conditions.
2. Considering the results of weight loss and i_{corr}, the corrosion rate of X80 steel in *R. palustris* TIE-1-inoculated medium under light conditions was approximately three times higher than that under dark conditions within 14 days.
3. The EN results under alternating light/dark conditions demonstrated that light stimulation promoted the transition from unstable localized corrosion to steady-state corrosion in the early stage of corrosion.
4. The photorespiratory of *R. palustris* TIE-1 played a crucial role in promoting MIC. Inhibiting photorespiratory chain significantly reduced the corrosion rate of X80 steel under light conditions, returning to levels observed under dark conditions.

CRediT authorship contribution statement

Yuntian Lou: Writing – original draft, Methodology, Investigation, Formal analysis. **Hao Zhang:** Methodology, Formal analysis. **Ziyu Li:** Methodology, Formal analysis. **Shaopeng Liu:** Formal analysis. **Weiwei Chang:** Formal analysis. **Hongchang Qian:** Formal analysis. **Xiangping Hao:** Formal analysis. **Dawei Zhang:** Writing – review & editing, Supervision, Methodology, Conceptualization.

Declaration of Competing Interest

The authors declare no competing financial interest.

Data availability

Data will be made available on request.

Acknowledgments

References

[1] A. Seyeux, S. Zanna, A. Allion, P. Marcus, The fate of the protective oxide film on stainless steel upon early stage growth of a biofilm, Corros. Sci. 91 (2015) 352–356.
[2] P. Jogdeo, R. Chai, S. Shuyang, M. Saballus, F. Constancias, S.L. Wijesinghe, D. Thierry, D.J. Blackwood, D. McDougald, S.A. Rice, E. Marsili, Onset of microbial influenced corrosion (MIC) in stainless steel exposed to mixed species biofilms from equatorial seawater, J. Electrochem. Soc. 164 (2017) C532.
[3] D. Wang, J. Liu, R. Jia, W. Dou, S. Kumseranee, S. Punpruk, X. Li, T. Gu, Distinguishing two different microbiologically influenced corrosion (MIC) mechanisms using an electron mediator and hydrogen evolution detection, Corros. Sci. 177 (2020) 108993.
[4] H.C. Flemming, E.D. van Hullebusch, T.R. Neu, P.H. Nielsen, T. Seviour, P. Stoodley, J. Wingender, S. Wuertz, The biofilm matrix: multitasking in a shared space, Nat. Rev. Microbiol. 21 (2023) 70–86.
[5] M. Moradi, S. Ye, Z. Song, Dual role of *Psudoalteromonas piscicida* biofilm for the corrosion and inhibition of carbon steel in artificial seawater, Corros. Sci. 152 (2019) 10–19.
[6] E.M. Suarez, K. Lepkova, B. Kinsella, L.L. Machuca, Aggressive corrosion of steel by a thermophilic microbial consortium in the presence and absence of sand, Int. Biodeterior. Biodegrad. 137 (2019) 137–146.
[7] Y. Ma, Y. Zhang, R. Zhang, F. Guan, B. Hou, J. Duan, Microbiologically influenced corrosion of marine steels within the interaction between steel and biofilms: a brief view, Appl. Microbiol. Biotechnol. 104 (2020) 515–525.
[8] D. Xu, T. Gu, D.R. Lovley, Microbially mediated metal corrosion, Nat. Rev. Microbiol. 21 (2023) 705–718.
[9] B. Chugh, Sheetal, M. Singh, S. Thakur, B. Pani, A.K. Singh, V.S. Saji, Extracell. Electron Transf. *Pseudomonas aeruginosa* Biocorrosion: A Rev. ACS Biomater. Sci. Eng. 8 (2022) 1049–1059.
[10] P.L. Tremblay, L.T. Angenent, T. Zhang, Extracellular electron uptake: among autotrophs and mediated by surfaces, Trends Biotechnol. 35 (2017) 360–371.
[11] T. Cui, H. Qian, Y. Lou, X. Chen, T. Sun, D. Zhang, X. Li, Single-cell level investigation of microbiologically induced degradation of passive film of stainless steel via FIB-SEM/TEM and multi-mode AFM, Corros. Sci. 206 (2022) 110543.
[12] H. Venzlaff, D. Enning, J. Srinivasan, K.J.J. Mayrhofer, A.W. Hassel, F. Widdel, M. Stratmann, Accelerated cathodic reaction in microbial corrosion of iron due to direct electron uptake by sulfate-reducing bacteria, Corros. Sci. 66 (2013) 88–96.
[13] L. Huang, Y. Huang, Y. Lou, H. Qian, D. Xu, L. Ma, C. Jiang, D. Zhang, Pyocyanin-modifying genes phzM and phzS regulated the extracellular electron transfer in microbiologically-influenced corrosion of X80 carbon steel by *Pseudomonas aeruginosa*, Corros. Sci. 164 (2020) 108355.
[14] Y. Hu, L. Huang, Y. Lou, W. Chang, H. Qian, D. Zhang, Microbiologically influenced corrosion of stainless steels by *Bacillus subtilis* via bidirectional extracellular electron transfer, Corros. Sci. 207 (2022) 110608.
[15] Z. Fang, Y.J. Tang, M.A.G. Koffas, Harnessing electrical-to-biochemical conversion for microbial synthesis, Curr. Opin. Biotechnol. 75 (2022) 102687.
[16] M. Soundararajan, R. Ledbetter, P. Kusuma, S. Zhen, P. Ludden, B. Bugbee, S. A. Ensign, L.C. Seefeldt, Phototrophic N_2 and CO_2 fixation using a *Rhodopseudomonas palustris*-H_2 mediated electrochemical system with infrared photons, Front. Microbiol. 10 (2019).
[17] R. Singh, T.O. Ranaivoarisoa, D. Gupta, W. Bai, A. Bose, Genetic redundancy in iron and manganese transport in the metabolically versatile bacterium *Rhodopseudomonas palustris* TIE-1, Appl. Environ. Microbiol. 86 (2020) e01057-01020.
[18] Y.J. Li, R. Wang, C.Y. Lin, S.H. Chen, C.H. Chuang, T.H. Chou, C.F. Ko, P.H. Chou, C.T. Liu, Y.H. Shih, The degradation mechanisms of *Rhodopseudomonas palustris* toward hexabromocyclododecane by time-course transcriptome analysis, Chem. Eng. J. 425 (2021) 130489.
[19] C.S. Harwood, Rhodopseudomonas palustris, Trends Microbiol. 30 (2022) 307–308.
[20] P.T. Ha, S.R. Lindemann, L. Shi, A.C. Dohnalkova, J.K. Fredrickson, M.T. Madigan, H. Beyenal, Syntrophic anaerobic photosynthesis via direct interspecies electron transfer, Nat. Commun. 8 (2017).
[21] G. Dong, Y. Chen, Z. Yan, J. Zhang, X. Ji, H. Wang, R.A. Dahlgren, F. Chen, X. Shang, Z. Chen, Recent advances in the roles of minerals for enhanced microbial extracellular electron transfer, Renew. Sustain. Energy Rev. 134 (2020) 110404.
[22] A. Bose, E.J. Gardel, C. Vidoudez, E.A. Parra, P.R. Girguis, Electron uptake by iron-oxidizing phototrophic bacteria, Nat. Commun. 5 (2014) 3391.
[23] K. Rengasamy, T. Ranaivoarisoa, R. Singh, A. Bose, An insoluble iron complex coated cathode enhances direct electron uptake by *Rhodopseudomonas palustris* TIE-1, Bioelectrochemistry 122 (2018) 164–173.
[24] Z. Li, W. Chang, T. Cui, D. Xu, D. Zhang, Y. Lou, H. Qian, H. Song, A. Mol, F. Cao, T. Gu, X. Li, Adaptive bidirectional extracellular electron transfer during accelerated microbiologically influenced corrosion of stainless steel, Communications, Materials 2 (2021) 67.
[25] C. Sun, Q. Yu, Z. Zhao, Y. Zhang, Extracellular electron uptake for CO2 fixation by *Rhodopseudomonas palustris* during electro-cultivation in darkness, Sci. Total Environ. 849 (2022) 157864.
[26] Y. Lou, C. Dai, W. Chang, H. Qian, L. Huang, C. Du, D. Zhang, Microbiologically influenced corrosion of FeCoCrNiMo0.1 high-entropy alloys by marine Pseudomonas aeruginosa, Corros. Sci. 165 (2020) 108390.
[27] R. Jia, J.L. Tan, P. Jin, D.J. Blackwood, D. Xu, T. Gu, Effects of biogenic H2S on the microbiologically influenced corrosion of C1018 carbon steel by sulfate reducing *Desulfovibrio vulgaris* biofilm, Corros. Sci. 130 (2018) 1–11.
[28] Z. Xu, T. Zhang, H. Wan, Y. He, J. Wang, R. He, H. Liu, Electrochemical investigation of the "double-edged" effect of low-dose biocide and exogenous electron shuttle on microbial corrosion behavior of carbon steel and copper in enriched seawater, Electrochim. Acta 476 (2024) 143687.
[29] Z. Li, A. Homborg, Y. Gonzalez-Garcia, P. Visser, M. Soleimani, A. Mol, The effect of ambient ageing on the corrosion protective properties of a lithium-based conversion layer, J. Electrochem. Soc. 170 (2023) 031504.

[30] A.M. Homborg, T. Tinga, X. Zhang, E.P.M. van Westing, P.J. Oonincx, J.H.W. de Wit, J.M.C. Mol, Time–frequency methods for trend removal in electrochemical noise data, Electrochim. Acta 70 (2012) 199–209.

[31] H. Qian, D. Zhang, Y. Lou, Z. Li, D. Xu, C. Du, X. Li, Laboratory investigation of microbiologically influenced corrosion of Q235 carbon steel by halophilic archaea *Natronorubrum tibetense*, Corros. Sci. 145 (2018) 151–161.

[32] D. Kampjut, L.A. Sazanov, The coupling mechanism of mammalian respiratory complex I, Science 370 (2020) eabc4209.

[33] M. Li, T. Zhu, R. Yang, Z. Wang, M. Liu, J. Yang, Carotenoids synthesis affects the salt tolerance mechanism of *Rhodopseudomonas palustris*, Front. Microbiol. 14 (2023) 1292937.

[34] T. Liu, S. Pan, Y. Wang, Z. Guo, W. Wang, Q. Zhao, Z. Zeng, N. Guo, *Pseudoalteromonas lipolytica* accelerated corrosion of low alloy steel by the endogenous electron mediator pyomelanin, Corros. Sci. 162 (2020) 108215.

[35] Z. Guo, X. Hui, Q. Zhao, N. Guo, Y. Yin, T. Liu, Pigmented *Pseudoalteromonas piscicida* exhibited dual effects on steel corrosion: inhibition of uniform corrosion and induction of pitting corrosion, Corros. Sci. 190 (2021) 109687.

[36] W. Bai, T.O. Ranaivoarisoa, R. Singh, K. Rengasamy, A. Bose, n-Butanol production by *Rhodopseudomonas palustris* TIE-1, Communications, Biology 4 (2021) 1257.

[37] X. Liu, L. Huang, C. Rensing, J. Ye, K.H. Nealson, S. Zhou, Syntrophic interspecies electron transfer drives carbon fixation and growth by *Rhodopseudomonas palustris* under dark, anoxic conditions, Sci. Adv. 7 (2021) eabh1852.

[38] H. Rui, H.P. Zhu, F.L. Niu, Y.G. Zhao, Y. Zhang, A.X. Yang, T. Zhou, Effect of LBE Corrosion on Surface Wettability of Ti3SiC2 at 450° C. Materials Science Forum, Trans Tech Publ, 2019, pp. 458–465.

[39] P. Li, L. He, X. Li, X. Liu, M. Sun, Corrosion inhibition effect of N-(4-diethylaminobenzyl) QUaternary Ammonium Chitosan for X80 pipeline steel in hydrochloric acid solution, Int. J. Electrochem. Sci. 16 (2021) 150929.

[40] S.J. Yuan, S.O. Pehkonen, Microbiologically influenced corrosion of 304 stainless steel by aerobic *Pseudomonas* NCIMB 2021 bacteria: AFM and XPS study, Colloids Surf. B: Biointerfaces 59 (2007) 87–99.

[41] Z. Cui, S. Chen, Y. Dou, S. Han, L. Wang, C. Man, X. Wang, S. Chen, Y.F. Cheng, X. Li, Passivation behavior and surface chemistry of 2507 super duplex stainless steel in artificial seawater: influence of dissolved oxygen and pH, Corros. Sci. 150 (2019) 218–234.

[42] P.S. Raghavan, A.A. Potnis, K. Bhattacharyya, D.A. Salaskar, H. Rajaram, Axenic cyanobacterial (Nostoc muscorum) biofilm as a platform for Cd(II) sequestration from aqueous solutions, Algal, Research 46 (2020) 101778.

[43] X. Cao, C. Li, B. Wu, M. Liang, Research of dynamic corrosion behavior, microstructure, and biocompatibility of Mg–Zn–Ca–Zr alloys in simulated body fluid solution induced by Zn element addition, Adv. Eng. Mater. 25 (2023) 2201402.

[44] M. Moradi, G. Ghiara, R. Spotorno, D. Xu, P. Cristiani, Understanding biofilm impact on electrochemical impedance spectroscopy analyses in microbial corrosion and microbial corrosion inhibition phenomena, Electrochim. Acta 426 (2022) 140803.

[45] G.J. Brug, A.L.G. van den Eeden, M. Sluyters-Rehbach, J.H. Sluyters, The analysis of electrode impedances complicated by the presence of a constant phase element, J. Electroanal. Chem. Interfacial Electrochem. 176 (1984) 275–295.

[46] C. Cardona, A.A. Torres, J.M. Miranda Vidales, J.T. Pérez, M.M. González Chávez, H. Herrera Hernández, L. Narváez, Assessment of dimethylbenzodiimidazole as corrosion inhibitor of austenitic stainless steel grade 316L in acid medium, Int. J. Electrochem. Sci. 10 (2015) 1966–1978.

[47] Y. Hou, C. Aldrich, K. Lepkova, B. Kinsella, Detection of under deposit corrosion in a CO_2 environment by using electrochemical noise and recurrence quantification analysis, Electrochim. Acta 274 (2018) 160–169.

[48] I.B. Obot, I.B. Onyeachu, A. Zeino, S.A. Umoren, Electrochemical noise (EN) technique: review of recent practical applications to corrosion electrochemistry research, J. Adhes. Sci. Technol. 33 (2019) 1453–1496.

[49] D.H. Xia, S.Z. Song, Y. Behnamian, Detection of corrosion degradation using electrochemical noise (EN): review of signal processing methods for identifying corrosion forms, Corros. Eng., Sci. Technol. (2016) 1–18.

[50] Z. Zhang, X. Li, Z. Zhao, P. Bai, B. Liu, J. Tan, X. Wu, In-situ monitoring of pitting corrosion of Q235 carbon steel by electrochemical noise: wavelet and recurrence quantification analysis, J. Electroanal. Chem. 879 (2020) 114776.

[51] Z. Li, A. Homborg, Y. Gonzalez-Garcia, A. Kosari, P. Visser, A. Mol, Evaluation of the formation and protectiveness of a lithium-based conversion layer using electrochemical noise, Electrochim. Acta 426 (2022) 140733.

[52] A. Homborg, P. Oonincx, J. Mol, Wavelet transform modulus maxima and holder exponents combined with transient detection for the differentiation of pitting corrosion using electrochemical noise, Corrosion 74 (2018) 1001–1010.

[53] F.H. Cao, Z. Zhang, J.X. Su, Y.Y. Shi, J.Q. Zhang, Electrochemical noise analysis of LY12-T3 in EXCO solution by discrete wavelet transform technique, Electrochim. Acta 51 (2006) 1359–1364.

[54] T. Zhang, Y. Shao, G. Meng, F. Wang, Electrochemical noise analysis of the corrosion of AZ91D magnesium alloy in alkaline chloride solution, Electrochim. Acta 53 (2007) 561–568.

[55] A.P. Wu, Y. He, S.Y. Ye, L.Y. Qi, L. Liu, W. Zhong, Y.H. Wang, H. Fu, Negative effects of a piscicide, rotenone, on the growth and metabolism of three submerged macophytes, Chemosphere 250 (2020) 126246.

[56] H. Schneider, B. Lai, J.O. Krömer, Interference of electron transfer chain inhibitors in bioelectrochemical systems, Electrochem. Commun. 152 (2023) 107527.